Equidistant fringe phase shift measurement by use of a trough integration method

Qin Wang
Xiao Wei Sun
Nanyang Technological University
School of Electrical and Electronic Engineering
Nanyang Avenue
Singapore 639798
E-mail: exwsun@ntu.edu.sg

Xijiang Yin
Advanced Materials Technology Center
Singapore Polytechnic
500 Dover Road
Singapore 139651

Abstract. A data processing method that extracts phase information through the integration of the trough part of the equidistant fringes was used in a phase shift measurement system based on a Michelson interferometer and a linear photo detector. The advantage of this method is substantiated theoretically and experimentally. The thermal drift and nonthermal drift of the system were observed and discussed. After deducting the error caused by the drifts, a 0.12-nm standard deviation was achieved in the displacement measurement with a movement range of several tens of nanometers. The measurement results of an antiparallel-aligned nematic liquid crystal (LC) cell and a polymer-dispersed liquid crystal (PDLC) cell by use of this system are also presented. [DOI: 10.1117/1.3028281]

Subject terms: interferometry; equidistant fringe; displacement measurement; phase shift; laser metrology.

Paper 080438R received Jun. 4, 2008; revised manuscript received Sep. 24, 2008; accepted for publication Sep. 26, 2008; published online Nov. 21, 2008.

1 Introduction

It is known that optical phase shift measurement is important for many applications. Extracting phase information from equidistant fringes is one approach to measure phase shift. Several data processing methods for extracting phase information from equidistant fringes have been reported, such as the Fourier transform method,[1,2] the peak position method,[3] and using the image matching algorithm.[4]

Previously, we applied a trough integration method (TIM) making use of equidistant fringes to measure the phase shift versus the driving voltage of a liquid crystal spiral phase plate.[5] This system is based on a Michelson interferometer and a linear photodetector array (LPDA).

In this paper, we present the technical details of this phase shift measurement system employing the trough integration method, including (1) theoretical substantiation about the trough integration method; (2) description of the experiment setup; (3) observation and discussion of the thermal drift and nonthermal drift; (4) experimental study of the system accuracy in measuring the displacement of the piezoelectric actuated mirror (PZT mirror); and (5) experimental results in the measurement of the displacement of the PZT mirror and the phase shift versus driving voltage of the antiparallel-aligned nematic liquid crystal (LC) and polymer-dispersed liquid crystal (PDLC) cells.

2 Trough Integration Method

The working principle of the measurement of phase shift by use of the equidistant fringe obtained through a Michelson interferometer with LPDA detector has been described in detail in Ref. 3. Here, we will focus on a new data processing method: the trough integration method.

A typical equidistant fringe curve obtained from a real system is shown in Fig. 1. We can see that the bottom of the equidistant curve has less distortion than the top part of the curve. In fact, this phenomenon is intrinsic.

In a real Michelson interferometer measurement system, the reference beam (R beam) and the object beam (O beam) are unavoidably mixed with some noises due to reflections from the surfaces of the optical components. Assuming that $A\exp[i(\omega t+f_1x)]$, $B\exp[i(\omega t+f_2x+\Delta)]$ and $C\exp[i(\omega t+\xi x)+\theta]$ represent the R beam, O beam, and noise, respectively, where all the parameters have their normal meanings, the intensity of the synthesized beam is

$$I(x)=A^2+B^2+C^2+2AB\cos(fx+\Delta)+2AC\cos(\xi x+\theta)+2BC\cos[(\xi-f)x-\Delta+\theta], \quad (1)$$

where $f=f_2-f_1$. For the sake of simplicity, assuming $A=B=1$, Eq. (1) can be written as

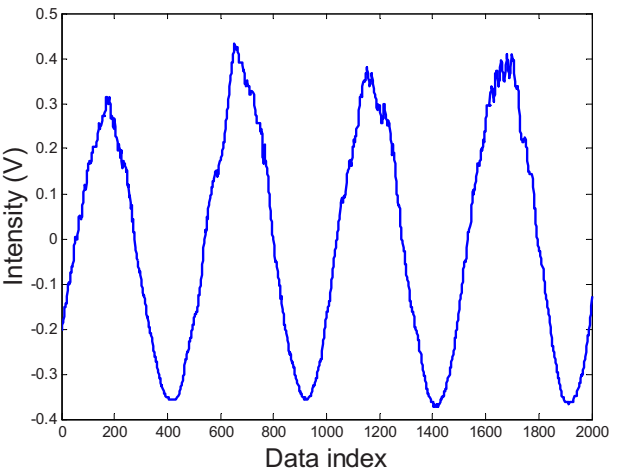

Fig. 1 A typical equidistant fringe curve obtained from a real system.

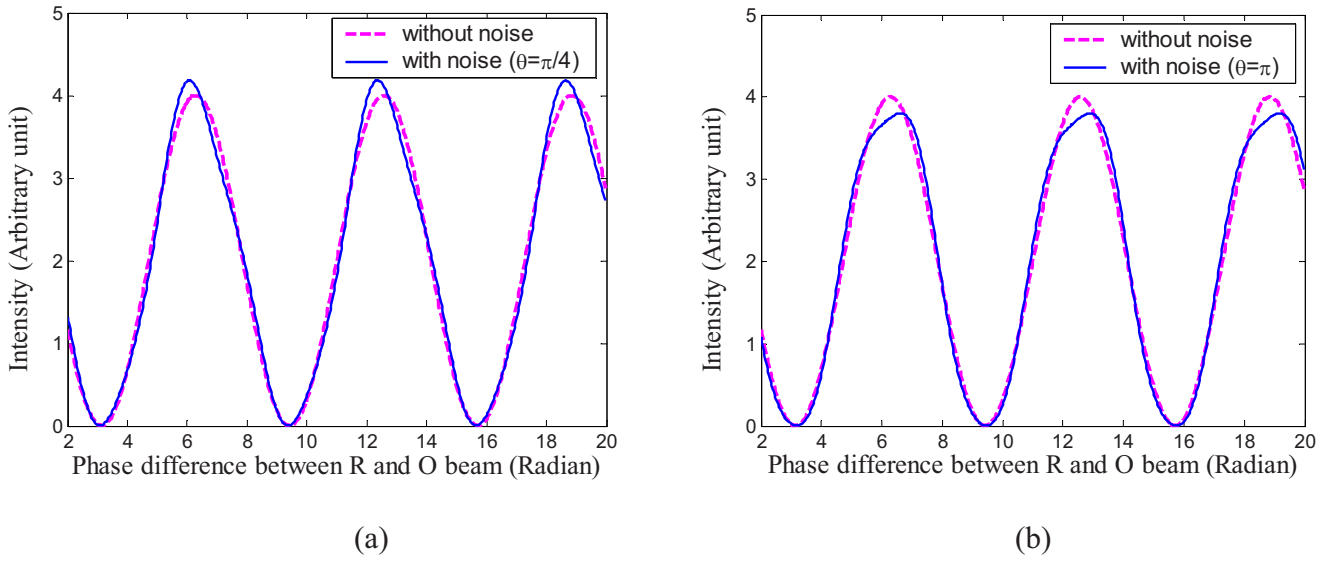

Fig. 2 Simulation results of the synthesized wave form of the R, O, and noise beams. Here the noise beam is assumed to be 0.5% of the R and O beams in intensity. Dashed lines are the synthesized wave forms without the noise beam; solid lines are the synthesized wave forms with the noise beam. (a) $\theta=\pi/4$, and (b) $\theta=\pi$, where θ represents the initial phase of the noise.

$$I(x) = 2 + C^2 + 2\cos(fx + \Delta) + 4C\cos\left(\frac{2\xi x - fx + 2\theta - \Delta}{2}\right)\cos\left(\frac{fx + \Delta}{2}\right). \quad (2)$$

The derivatives of $I(x)$ at the antiphase position $x=\{[(2n+1)\pi-\Delta]/f\}$ and in-phase position $x=(2n\pi-\Delta)/f$ of the R and O beams can be deduced from Eq. (2) as

$$\left.\frac{dI}{dx}\right|_{x=[(2n+1)\pi-\Delta]/f} = 2fC\cos\left[\frac{(2\xi-f)x + 2\theta - \Delta}{2}\right]$$

$$\left.\frac{dI}{dx}\right|_{x=(2n\pi-\Delta)/f} = 2(2\xi-f)C\cos\left[\frac{(2\xi-f)x + 2\theta - \Delta}{2}\right], \quad (3)$$

where n is an integer. For a real system, the noise with frequency $\xi>f$ is more significant than the noise with frequency $\xi<f$, so we have

$$\left|\left.\frac{dI}{dx}\right|_{x=(2n+1)\pi-\Delta/f}\right| < \left|\left.\frac{dI}{dx}\right|_{x=2n\pi-\Delta/f}\right|,$$

which means that the minimum points of the fringe curve represents the antiphase points more truthfully in comparison with the maximum points of the curve representing the in-phase points.

The factor of $\cos[(fx+\Delta)/2]$ in Eq. (2) is equal to zero at the antiphase points, while it reaches the maximum at the in-phase points, which means that the signal is less affected by the noise at the troughs in comparison with the crests.

Intuitively, Fig. 2 shows a simulation to illustrate the noise effect on the troughs and crests of a synthesized beam. In the unitless simulation, we used $A^2=B^2=1$, $C^2=0.05$, $f=3$, $\xi=10$, $\Delta=5/8\pi$, and $\theta=1/4\pi$ and $\theta=\pi$ for Figs. 2(a) and 2(b), respectively. The dashed and solid lines represent the fringe wave forms without and with the noise, respectively. It can be seen clearly that there are only very small discrepancies between the dashed lines and solid lines at the troughs, while there are considerable discrepancies at the crests.

Thus, the crest of the fringe curve is much more distorted in comparison with the trough due to the existence of noises in a real system. Hence, it is more accurate to use the minimum points of equidistant fringe waveforms to determine the position of the waveform than using the maximum points. We call this method the minimum position method (MPM).

The TIM we introduced here is more accurate compared to MPM. In fact, although the trough part is less affected by the noise, there is still discrepancy between the antiphase point and the minimum point due to the noises. We found the effect caused by the noise can be reduced to a considerable extent through the integration process as described here.

Figure 3 shows an enlarged part of the wave form in Fig. 2(a). The dashed and solid lines represent the fringe wave forms without noise and with noise, respectively. Draw an arbitrary horizontal line AE (parallel to the x axis), which intersects with the noise-containing curve at A and E. The integration level τ denotes the vertical coordinate of the line AE. C is the minimum point of the noise-containing curve, and m_1 and m_2 are the coordinates of A and E, respectively. $ABDE$ is the rectangle formed with its sides parallel to one x and y axes, respectively.

In a real system, the frequency of noise ξ is generally higher than the deference frequency of the O beam and R beam f. Therefore, the effect of noise may be deducted through integration over a range that is some multiple of the period of noise. This integration range should be within the trough part of the wave form where it is less affected by the noise. And the coordinates of the trough position

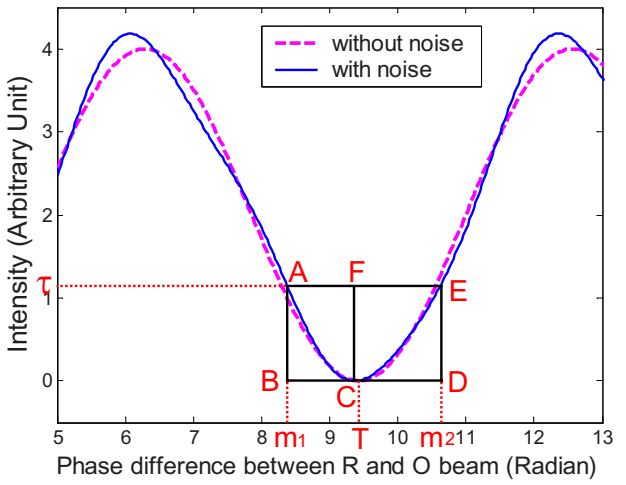

Fig. 3 Diagram for introducing the trough integration method.

$Ti(\tau,\theta)$, which is a function of τ and θ (the initial phase angle of noise), can be determined by a weighted average as

$$Ti(\tau,\theta)=\left(m_1+\frac{S_{ABC}}{S_{ABCF}}+m_2-\frac{S_{CDE}}{S_{CDEF}}\right)\Big/2, \tag{4}$$

where S_{ABC} and S_{CDE} represent the areas of the triangle-like shape ABC and CDE, respectively, which can be determined through integration calculation, and S_{ABCF} and S_{CDEF} represent the areas of the rectangles of $ABCF$ and $CDEF$, respectively.

Figure 4 shows the curve of the"error of TIM" versus the integration level τ. The error of TIM is defined as

$$\frac{1}{360}\sum_{\theta=1\ \mathrm{deg}}^{360\ \mathrm{deg}}(|Ti(\tau,\theta)-T|),$$

where T denotes the actual coordinate of the antiphase point, i.e., the minimum point of the curve without noise. So the error of TIM means the discrepancy between the values obtained by Eq. (4) and T averaged over θ. The dotted line indicates the level of the "error of MPM," which is defined as

$$\frac{1}{360}\sum_{\theta=1\ \mathrm{deg}}^{360\ \mathrm{deg}}(|Tm(\theta)-T|),$$

where $Tm(\theta)$ denotes the coordinates of the minimum point of the noise-containing curve, which is a function of θ. So the error of MPM means the discrepancy between the coordinates of the minimum point of the solid line and T averaged over θ.

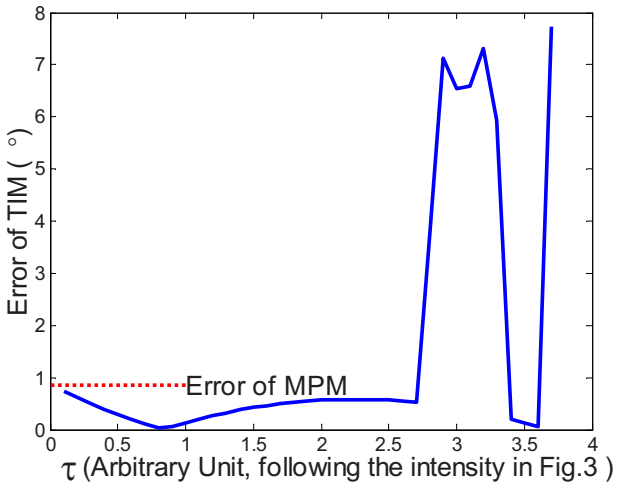

Fig. 4 Error of TIM versus integration level τ.

It can be clearly seen from Fig. 4 that there is a minimum on the curve in between $\tau=(0.5,1)$, where the error of TIM is considerably smaller than the error of MPM. It is worth noting that the dramatic increase of the error of TIM between $\tau=(2.5,3)$ reflects the conclusion from Eq. (2) that the distortion of the wave form is increased with the increasing of τ, and this effect is further magnified due to the fringe curve starting to become less steep in this specific region of τ.

Although the noise with a single frequency is assumed in the simulation shown in Fig. 4, the conclusion should not lack its generality when there is a combination of noises with different frequencies. By choosing a proper value of τ, more accurate measurement can be achieved by use of the TIM in comparison with the MPM.

As long as the coordinates of the trough position are determined, the phase shift can be calculated as

$$\text{Phase shift (deg)}=\frac{d}{p}\times 360\ \text{deg}, \tag{5}$$

where d represents the difference between the coordinates of the trough positions in two wave forms acquired in tandem, and p represents the period of the fringe curve. For determination of the period of the fringe, at least two troughs should be included in each wave form.

Compared with other methods, obviously, the trough integration method and the minimum position method can avoid the measurement error arising from the truncation of a fringe wave form, the high distortion in the top part of a fringe curve, and the nonlinear response of the detector, from which the measurement accuracy of other methods suffers. Moreover, unlike the other methods where more than ten periods of fringes are required, only two periods of the fringe signal are sufficient in TIM and MPM. Thus, more pixels on LPDA can be available for one period of the fringe, which is another merit to the precise determination of the trough position.

3 Experiment Setup

A schematic diagram and photo of the experiment setup are shown in Figs. 5(a) and 5(b), respectively. The laser used in the system is a 500:1 linearly polarized He-Ne laser (Newport Co.) with output power of 4 mW, operating at 632.8 nm wavelength. The magnification of the objective is 40; the pin hole is 25 μm in diameter. Lens 1 is a flat-concave lens with antireflection coating and a focus length of 20 cm. The broadband nonpolarizing beamsplitting cube (Model BS016, Thorlabs) is coated with an antireflection layer.

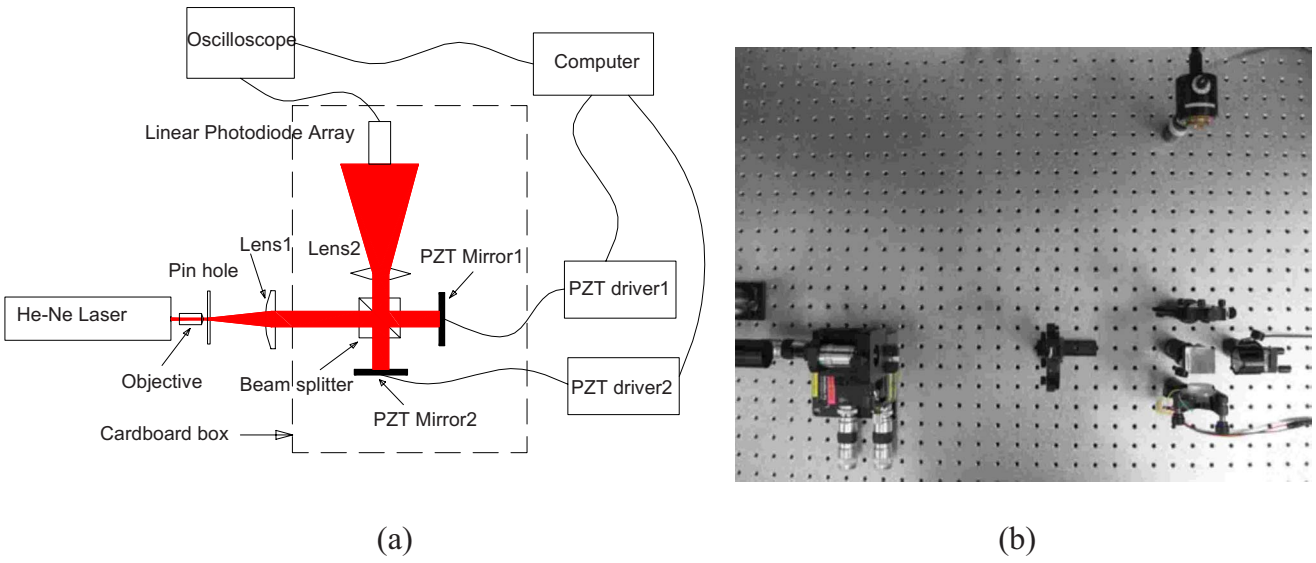

Fig. 5 (a) Diagram of the experiment setup. (b) Photo of the experiment setup.

The mirrors are broadband metallic mirrors with $\lambda/10$ surface flatness (Model 10D20, Newport). One of the mirrors is actuated by the PZT (Model FK-18515, Newport), which is driven by a function generator (Model Agt33250A, Agilent Co.). Another mirror is actuated by another PZT, which is driven by a voltage amplifier (Model NV40/3S, Piezosystem Jena).

Lens 2 is a concave lens with a focus length of 5 cm without antireflection coating. The LPDA (Optiscience Co.) has 1000 pixels, with a pitch of 7 μm. The scanning frequency of the LPDA is 362.3 Hz. The amplitude of the fringe signal detected in the experiment is around 790 mV. The signal from the LPDA is connected to an oscilloscope (Model Agt1541A, Agilent Co.), which can work in average mode, i.e., to display the averaging signal of a number of wave forms acquired in sequence. The data of the waveform displayed on the oscilloscope is then acquired by a computer through a GPIB port (NI USB GPIB).

The system was mounted on an optical table inside a 10,000-class clean room. During the measuring process, the air conditioner was shut down to reduce the vibration caused by air flow, and the interferometer parts [indicated with dashed line in Fig. 3(a)] were covered by a cardboard box with a small hole cut for the propagation of the laser beam.

The structure of the setup is similar to that used in Ref. 3. The only difference is the additional Lens 2 in our system, which is for magnifying the laser beam. Since the laser beam possesses a Gaussian intensity profile and a spherical wavefront, Lens 2 ensures that only the central part of the laser beam, which is a better approximation to a plane wave, is acquired. This helps to improve the uniformity of the pitches of the interference fringe and the irradiance shining on the LPDA.

The software for the measurement system is composed of two parts. The first part, written in microsoft Visual Basic, is for operation control and data acquisition, which includes setting the parameters of the oscilloscope, PZT driving signal generation, and wave form data acquisition. The second part, written in MATLAB, is dedicated to the data processing for extracting the results of the phase shift. The trough integration method is used in the data processing. It was found experimentally that the measurement results with the best standard deviation could be obtained when τ is at the level of one-fifth of the wave form's amplitude. The oscilloscope is therefore set to show one-fifth of the total amplitude only for increasing the vertical resolution. A typical acquired wave form is shown in Fig. 6. The total index number shown in the figure is not equal to the total pixel number of the LPDA, because the data size of the wave form is determined by the output buffer size of the oscilloscope.

4 Experimental Results and Discussions

This system was used to measure the displacement of the piezoelectric-actuated mirror (Model FK-18515, Newport). Figure 7 shows the measurement result. The hysteresis of the PZT can be clearly seen. The average number of the

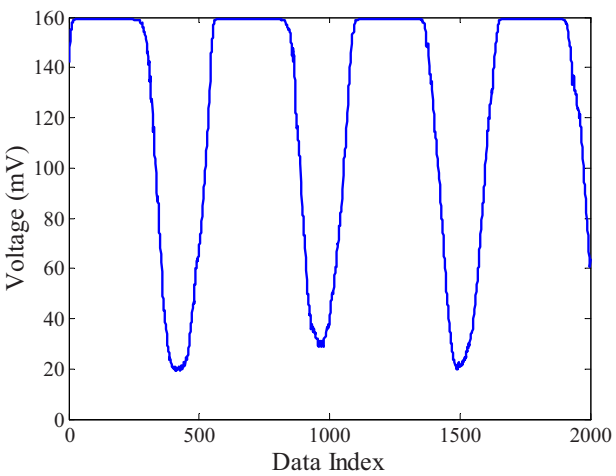

Fig. 6 The wave form acquired in the trough integration method.

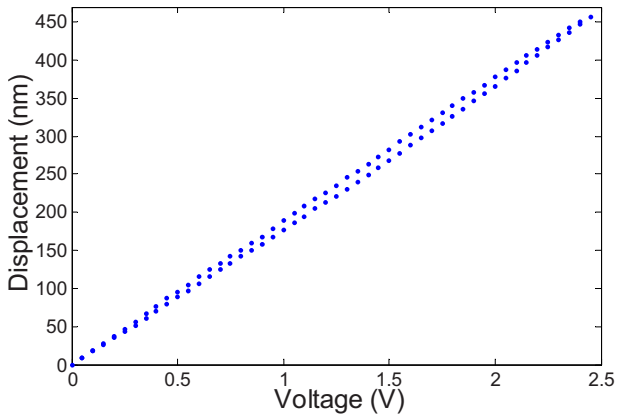

Fig. 7 Displacements measured clearly show the hysteresis of the PZT.

oscilloscope is set at 32, which means that the wave form displayed on the oscilloscope is an average of 32 scans from the LPDA; the duration of the measurement is 45 s, which includes the data acquiring time and the intervals between successive acquisitions. To evaluate the measurement accuracy of the system, the effect caused by thermal drift and nonthermal drift cannot be ignored.

4.1 *Observation of Thermal Drift and Nonthermal Drift*

The measurement of the drift is carried out without any driving signal applied to the PZT mirrors. Figure 8(a) shows the drift of the system measured in a period of 10 h. The temperature was recorded at the same time using a temperature monitor (Model STC 200, Instec Co.). The temperature sensor contacted the metal stage of the optical table within the area of the interferometer part. The temperature profile is shown in Fig. 8(b). It can be seen clearly that the phase drift follows a pattern similar to the temperature fluctuation. It is worth noting that there is a lag between the temperature fluctuation and the response of the phase drift, which is probably because the actual temperature has to be rounded due to the limited resolution (0.1 °C) of the temperature monitor. It can also be seen that the amplitude of the phase drift is not proportional to the amplitude of the temperature fluctuation, which means that the drift is not solely caused by temperature change. Nonthermal drift also exists.

The nonthermal drift mainly comes from the flow and creep of materials under mechanical stresses. In the experiment setup, all components are fixed by screws, so the stress undoubtedly exists. Figure 9(a) shows the measurement immediately after aligning the optical system. Since all the screws were locked shortly before the measurement, a remarkable drift speed in the beginning was observed; it then decayed slowly. The drift speed affected by the temperature fluctuation can also be clearly seen by comparing with the temperature profile as shown in Fig. 9(b). Again, there is a lag between the temperature change in Fig. 9(b) and the corresponding phase shift shown in Fig. 9(a). The reason for this phenomenon is the same as stated earlier.

4.2 *Evaluation of the Measurement Accuracy*

From the proceeding observations, it can be seen that it is not easy to control the drift speed within a very low level, because superior precision temperature control and special design of mechanics have to be involved. On the other hand, with the existing thermal drift and nonthermal drift, it is still possible to evaluate the accuracy of the measurement method. This is because in a short time interval—less than one minute, for instance—both the thermal drift and the nonthermal drift can be approximately regarded as changing linearly with time, and thus the measurement deviation caused by drift can be deducted through linear curve fitting.

To evaluate the accuracy, the same PZT mirror in the hysteresis measurement was used, but the measurement was carried out in a smaller displacement range. The measurement results with the oscilloscope setting at different average numbers are shown in Fig. 10. The total duration times for all the four measurements were made the same (45 s) by setting appropriate time intervals between two successive wave form acquisitions in the operation control program.

It can be seen from Fig. 10 that with the increase of the

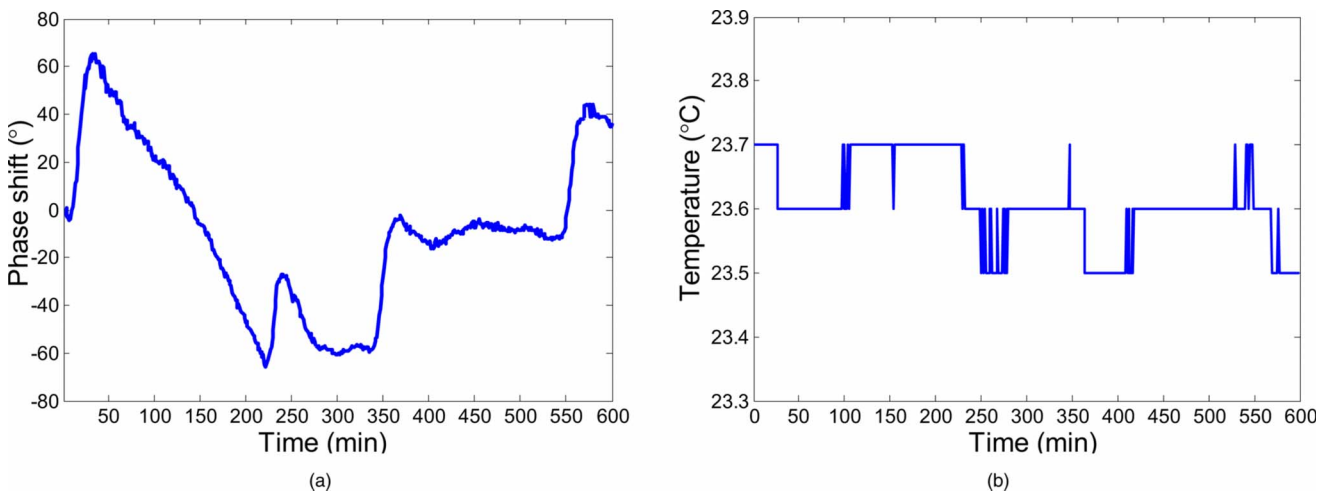

Fig. 8 (a) Drift measured in a period of 10 h. (b) Temperature profile recorded synchronously.

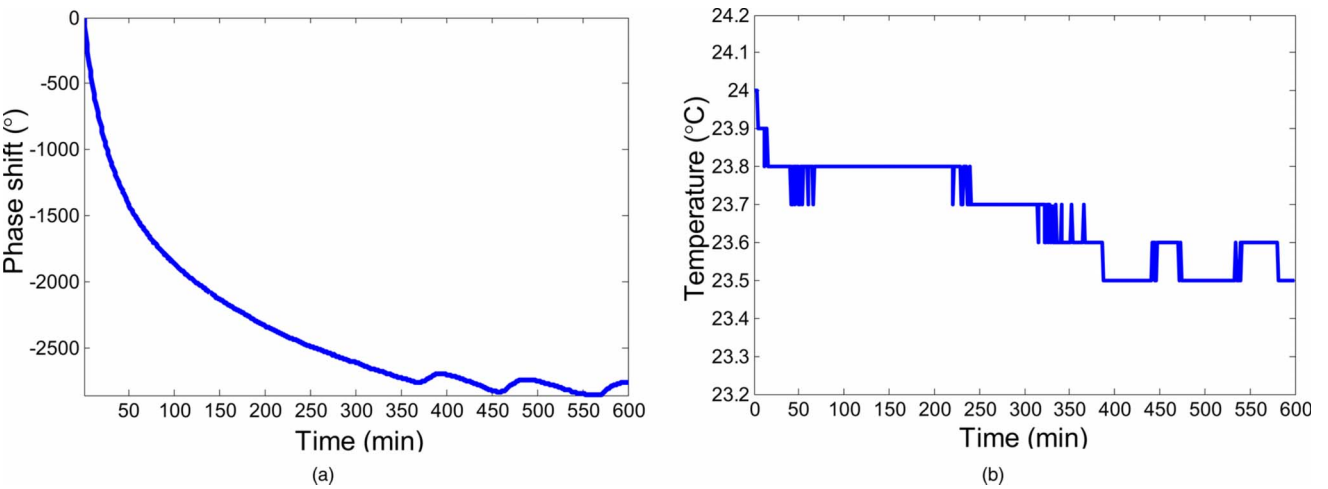

Fig. 9 (a) Drift measured in a period of 10 h shortly after the alignment of the optical system. (b) Temperature profile recorded synchronously.

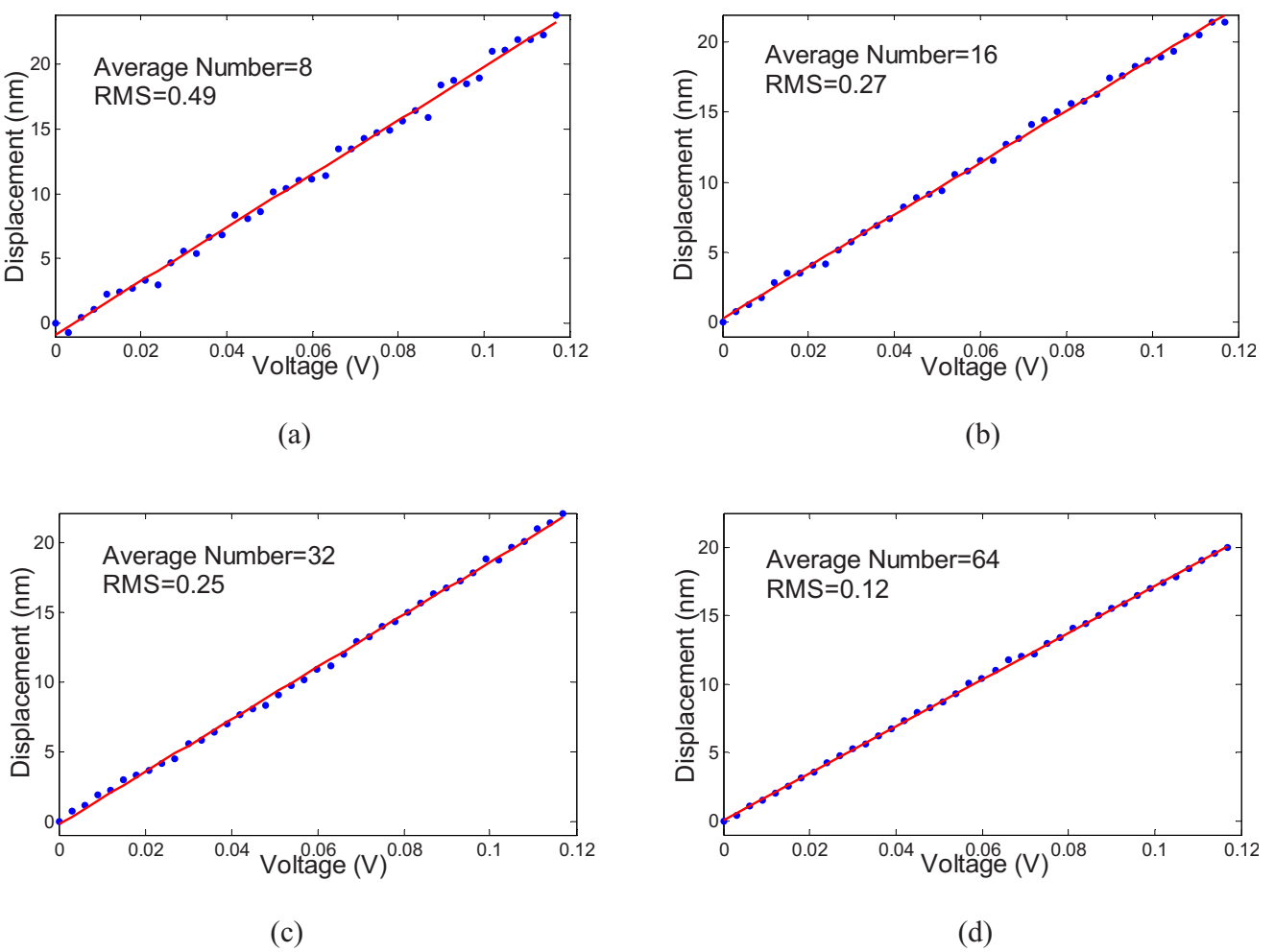

Fig. 10 The displacement versus the driving voltage of the Newport FK-18515 PZT mirror measured under conditions of different average numbers of the oscilloscope: (a) average number=8; (b) average number=16; (c) average number=32; and (d) average number=64.

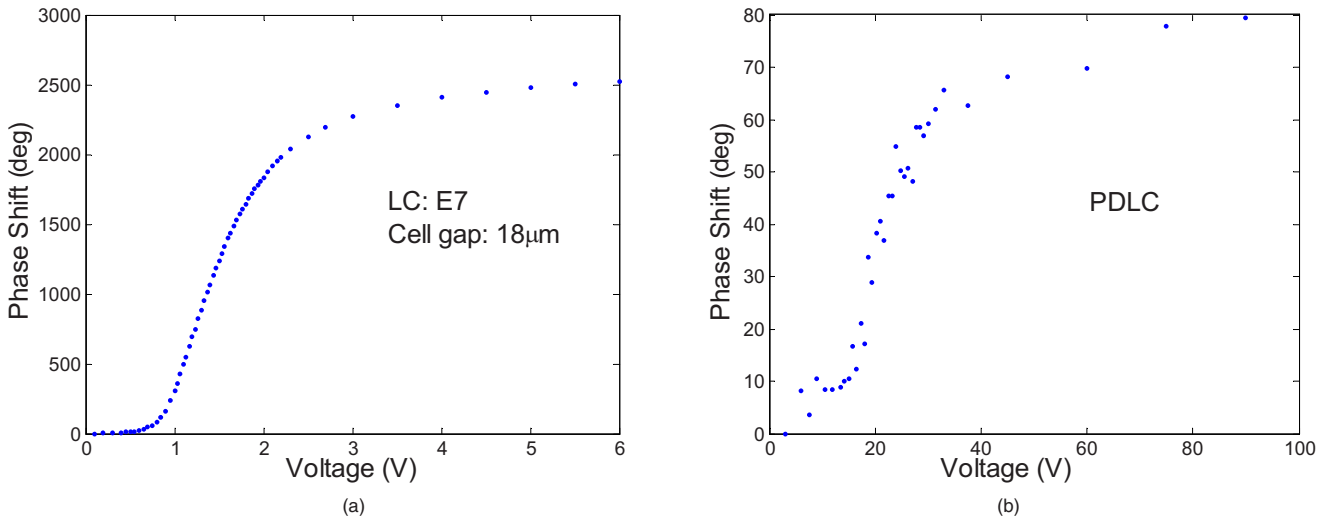

Fig. 11 The phase shift versus the driving voltage of a (a) liquid crystal spiral phase plate and (b) PDLC cell measured by the system.

average number, the standard deviation of the measured data (RMS values shown in the figures) is decreased. This result can be expected because the effect of the random noise decreases with the increasing of the average number. When further increasing the average number above 64, no explicit improvement of standard deviation was observed, which means that the influence of the random noise had been reduced to its limit.

As shown in Fig. 10(d), a remarkable standard deviation of 0.12 nm was achieved by the trough integration method. By comparison, the minimum position method was also used to process the same wave form data, and the standard deviation obtained is 0.87 nm, indicating the effectiveness of TIM.

In these experiments, the Agt33250A function generator is used to drive the PZT, and each voltage increment is 3 mV. As the specification of this function generator indicates that the output voltage precision is ± 1 mV, to avoid any deviation caused by the driving voltage, another PZT mirror with smaller displacement/voltage ratio was investigated. However, no explicit improvement of standard deviation was observed, and therefore the deviation caused by the driving voltage in the experiments should be small.

4.3 *Measurement of Phase Shift Versus Driving Voltage of Nematic LC and PDLC*

The system was applied in the determination of the phase shift of a nematic LC phase retarder. The measurement result for one nematic LC phase retarder is shown in Fig. 11(a), which was found helpful in the driving of liquid crystal spiral phase plate.[5] When making this measurement, the LC cell is inserted in one of the arms of the interference system, with the rubbing direction of an antiparallel rubbed LC cell in parallel with the polarization of the laser beam.

A polymer-dispersed liquid crystal (PDLC) cell sample fabricated in our lab was also investigated by this system. The phase shift of the PDLC cell cannot be measured by any retardation measurement systems, such as a polarimeter, because the optical paths of PDLC cells are isotropic in different polarization directions. The measurement result for the PDLC cell is shown in Fig. 11(b). It can be seen that the deviation of the measured data is much bigger than that for the nematic LC cell. This should be caused by the strong scattering of the LC droplets inside the PDLC cell. Despite the strong noise, the threshold voltage and saturation voltage can still be estimated.

4.4 *Approaches to Further Improve the Measurement Accuracy*

Although good experimental results have been obtained with the system using the trough integration method, there is still room for further improving the measurement accuracy. One approach is to control the drift speed, and this can be achieved only through ultraprecision temperature control and special designed mechanical parts. Another approach is to reduce the multireflection noise beam, which is possible to achieve through some special design of the optics of the system. The third approach is to use USB a port LPDA with larger pixel number and higher scan frequency, which will help to determine the trough position more precisely and improve the measurement speed.

5 Conclusions

In summary, a trough integration method for data processing in the measurement of equidistant fringe phase shift is proposed. An experiment setup was built, and the program for the trough integration method was developed and applied in the measurement. The advantage of this method is substantiated experimentally. Both thermal drift and nonthermal drift of this system are explicitly observed. Experimental results of the measurement of the displacement of the PZT mirror and phase shift of LC and PDLC cell versus driving voltage by use of this system are presented.

References

1. S. Nakadate, "Phase detection of equidistant fringes for highly sensitive optical sensing. I. Principle and error analyses," *J. Opt. Soc. Am. A* **5**, 1258–1264 (1988).
2. S. Nakadate, "Phase detection of equidistant fringes for highly sensitive optical sensing. II. Experiments," *J. Opt. Soc. Am. A* **5**, 1265–1269 (1988).

3. J. H. Yi, S. H. Kim, Y. K. Kwak, and Y. W. Lee, "Peak movement detection method of an equally spaced fringe for precise position measurement," *Opt. Eng.* **41**(2), 428–434 (2002).
4. Z. Wang, M. S. Graca, P. J. Bryanston-Cross, D. J. Whitehouse, "Phase-shifted image matching algorithm for displacement measurement," *Opt. Eng.* **35**(8), 2327–2332 (1996).
5. Q. Wang, X. W. Sun, P. Shum, and X. J. Yin, "Dynamic switching of optical vortices with dynamic gamma-correction liquid crystal spiral phase plate," *Opt. Express* **13**, 10285–10291 (2005).

Qin Wang received his PhD from the School of Electrical and Electronic Engineering, Nanyang Technological University, Singapore, in 2008. His research interests include liquid crystal devices, optical phase shift measurement, optical vortex, and dye-sensitized solar cells. He is currently a research fellow at Nanyang Technological University, Singapore.

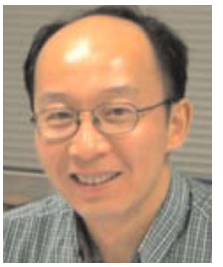

Xiao Wei Sun is currently an associate professor at the School of Electrical and Electronic Engineering, Nanyang Technological University, Singapore. He received his PhD from the Hong Kong University of Science and Technology in 1998. His current research interests include nanotechnology, display technologies, and ZnO nanodevices.

Xijiang Yin is currently director of the Advanced Materials Technology Centre (AMTC), Singapore Polytechnic. He received his PhD from the University of Birmingham, UK, in 1992. His current research interests include flat panel display technology, surface engineering, and thin film solar cell technology.